Three-Dimensional Reconstruction and Analysis of All-Solid Li Ion Battery Electrode

Using Synchrotron Transmission X-ray Microscopy Tomography

Tianyi Li[1], Huixiao Kang[1], Xinwei Zhou[1], Cheolwoong Lim[1], Bo Yan[2], Vincent De

Andrade[3], Francesco De Carlo[3], and Likun Zhu[*,1]

[1]Department of Mechanical Engineering, Indiana University–Purdue University

Indianapolis, Indianapolis, Indiana 46202, USA

[2]School of Materials Science and Engineering, Shanghai Jiao Tong University,

Shanghai, 200030, China

[3]Advanced Photon Source, Argonne National Laboratory, Argonne, Illinois 60439,

USA

[*]Corresponding Author:

Likun Zhu

Department of Mechanical Engineering

Indiana University Purdue University Indianapolis

723 W. Michigan Street, Room SL 260 L

Indianapolis, IN 46202

Phone: 1-317-274-4887

Fax: 1-317-274-9744

* Email: likzhu@iupui.edu

_____

Abstract

A synchrotron transmission X-ray microscopy tomography system with a spatial resolution of 58.2 nm at the Advanced Photon Source was employed to obtain three-dimensional morphology data of all-solid Li ion battery electrodes. The three-phase electrode was fabricated from a 47:47:6 (wt%) mixture of $Li(Ni_{1/3} Mn_{1/3} Co_{1/3})O_2$ as active material, $Li_{1.3}Ti_{1.7}Al_{0.3}(PO_4)_3$ as Li-ion conductor, and Super P carbon as electron conductor. The geometric analysis show that particle-based all-solid Li ion battery has serious contact interface problem which significantly impact the Li ion transport and intercalation reaction in the electrode, leading to low capacity, poor rate capability and cycle life.

2

1
2
3
4
5
6
7
8
9
10
11
12
13
14
15
16
17
18
19
20
21
22
23
24
25
26
27
28
29
30
31
32
33
34
35
36
37
38
39
40
41
42
43
44
45
46
47
48
49
50
51
52
53
54
55
56
57
58
59
60

In recent years, research on all-solid Li ion batteries (LIBs) has increased considerably due to raised concerns relating to safety hazards such as the solvent leakage and flammability of liquid electrolytes used for commercial LIBs[1-6]. All-solid LIBs use high Li ion conducting solid electrolytes that do not carry the safety burdens of liquid electrolytes and are more effective. In addition, all-solid LIBs can increase the energy density of the entire battery pack by reducing the need for auxiliary systems such as safety monitoring systems[7]. However, even with the highly ionic conductive solid electrolytes, it has been a struggle for an all-solid LIB to obtain similar specific capacity, rate capability, and cycle life to those of a liquid electrolyte LIB. Studies conclude that these issues arise from the solid electrolyte's inability to interface with the solid active materials, which is mainly due to the volume change of electrode materials during charge and discharge processes[8-10]. Some strategies have been proposed to address the interface problem, such as surface coating[11-12], zero strain electrode materials [13-14], and hybrid electrolyte [9, 15]. However, the interface problem has not been completely solved, especially in a three-dimensional (3D) particles-based electrode. Therefore, it is necessary to investigate the interface between active materials and solid electrolyte in a realistic microstructure of all-solid LIB electrode to understand the poor performance of all-solid LIBs.

In the past several years, some virtualization technologies have been developed to obtain the real configuration of LIB electrode microstructures. For instance, focused ion beam scanning electron microscope (FIB-SEM)[16-18] and nano-computed

3

tomography (CT)[19-21] have been used to reconstruct the 3D microstructure of liquid

electrolyte LIB electrodes. Most of the 3D microstructures obtained by these two

technologies consist of two phases, active material and pore + carbon-binder matrix.

Recently, some techniques have been developed to identify the pore phase and carbon-

binder matrix phase[22-23]. The all-solid LIB electrode consists of three phases, active

material, solid electrolyte and pore. Both active material and solid electrolyte are solid

particles in the electrode. To reconstruct the microstructure of all-solid LIB electrode,

these two solid phases need to be identified. To this end, the 3D microstructure of all-

solid LIB electrode has not been investigated. The only similar work was done by Wang

et al. at Brookhaven National Laboratory[24-25]. In their work, the 3D morphology of

$LiCoO_2/Li(Ni_{1/3}Mn_{1/3}Co_{1/3})O_2$ (LCO/NMC) composite cathode electrode has been

measured using FIB-SEM tomography and transmission X-ray microscopy (TXM)

tomography. EDS mapping was used in FIB-SEM tomography to identify LCO and

NMC particles and TXM measurements were taken at X-ray energies that can provide

clear contrast between LCO and NMC particles.

The objective of this paper is to investigate the realistic microstructure of all-solid LIB

electrode to better understand the interface between active materials and solid

electrolyte using synchrotron TXM tomography technique with high spatial resolution.

Although FIB-SEM tomography enables the identification of solid particles with EDS

mapping, it was not chosen in this study due to the time consumption and difficulty of

operation[18]. In this work, NMC was selected as the active material, $Li_{1.3}Ti_{1.7}Al_{0.3}(PO_4)_3$

4

(LTAP) was selected as the solid electrolyte and Super P carbon was used as the electron conductor. The electrodes were manufactured under two different pressures to adjust the porosity and particle contact. We reconstructed the porous microstructures of all-solid electrodes to examine geometric characteristics by employing synchrotron TXM at the Advanced Photon Source (APS) of the Argonne National Laboratory (ANL). Based on the tomographic data, the interface problem was discussed in this paper.

In this work, NMC powders were from Umicore, Brussels, Belgium; super-P carbon black (C65, TIMCAL Ltd.) was from MTI, Richmond, CA; LTAP was synthesized in our lab based on a modified method shown in literature[26]. Briefly, lithium carbonate (Li_2CO_3), aluminum oxide (Al_2O_3), titanium dioxide (TiO_2), and ammonium dihydrogen phosphate ($(NH_4)_2H_2PO_4$) purchased from Sigma Aldrich were ground and heated in a platinum crucible at 1652 ˚F for 2 h. The resulting material was ball milled for 6 h and re-heated at 1652 ˚F for 2 h. The powder was subjected to ball milling for 12 h to obtain the final LTAP powder. The final powder was dried at 120 ˚C for 24 h to remove any attached water molecules. The all-solid electrode was made from a 47:47:6 (wt %) mixture of NMC as active material, LTAP as Li-ion conductor, and Super P carbon as electron conductor. The electrode was pressed under two conditions: 700 psi and 1300 psi. We also made a LTAP only solid electrolyte pressed under 1300 psi, which can be used as the separator for all-solid LIBs. The detailed fabrication method is shown in our previous publication[9].

5

1
2
3
4
5
6
7
8
9
10
11
12
13
14
15
16
17
18
19
20
21
22
23
24
25
26
27
28
29
30
31
32
33
34
35
36
37
38
39
40
41
42
43
44
45
46
47
48
49
50
51
52
53
54
55
56
57
58
59
60

A synchrotron TXM at beamline 32-ID-C at the APS of ANL was employed to obtain morphological data of the electrodes. A sharp razor was used to break the electrode samples to small pieces. One piece with a sharp wedge was selected and mounted to the rotation stage of the TXM system. High energy level X-ray (8 keV) from the beamline was able to capture the projected X-ray images with 2 s exposure time at each 0.25° rotation increments over 180°. Normalized transmission of NMC and LTAP at 8 keV is shown in Figure 1a. The result shows that 8 keV X-ray can provide a good contrast between NMC and LTAP, which allows accurate segmentation by simple threshold. Image processing method was inherited and improved based on our previous studies on graphite, LCO and NMC electrodes[27-29]. ImageJ was used to remove system errors of the projection images based on flat field images. TomoPy was used to transform the projection image dataset into 3D reconstruction data with $58.2 \times 58.2 \times 58.2 \text{ nm}^3$ voxel size.
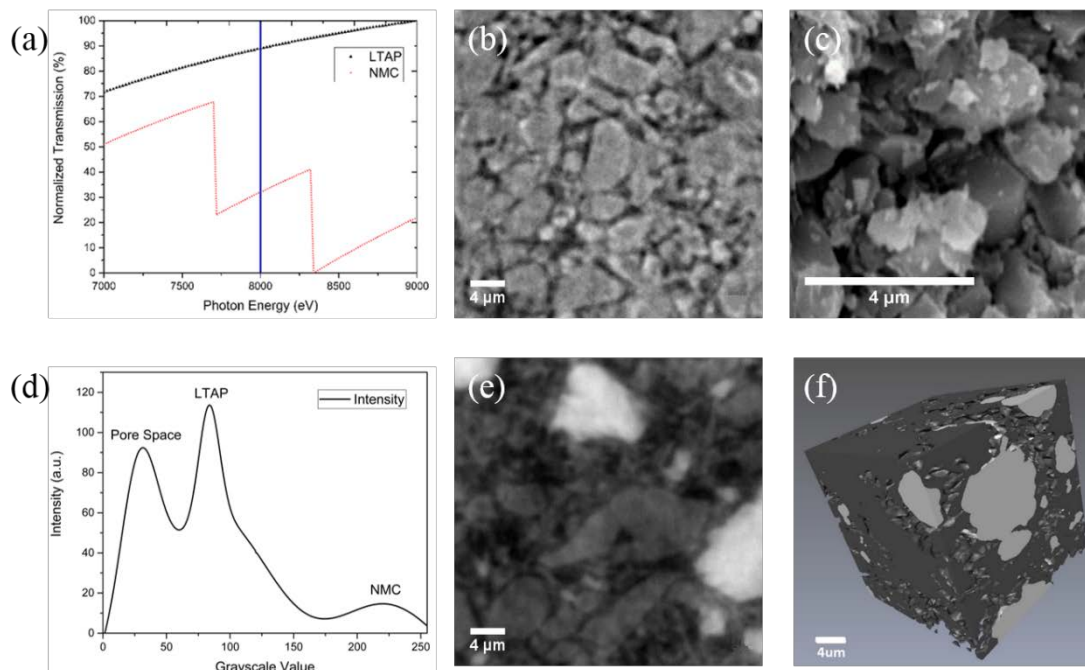
6

Figure 1. (a) Calculated X-ray transmission of LTAP and NMC based on tabulated values. 2D CT image (b) and SEM image (c) of a LTAP separator. (d) Grayscale histogram of a 2D CT image shown in (e). (e) 2D CT image of a 700 psi all-solid electrode. (f) 3D reconstruction of a 700 psi all-solid electrode. All the scale bars are 4 μm.

Figure 1b shows a reconstructed 2D slice image of the LTAP separator pressed under 1300 psi, where the gray phase is LTAP and the black phase is pore. A SEM image of the LTAP separator is shown in Figure 1c. Figure 1e shows a representative reconstructed 2D slice image of 700 psi all-solid electrode. Compared to our previous X-ray CT images of liquid electrolyte electrodes, such as LCO and NMC[27-28], the all-solid electrode has three phases to be distinguished. As shown in Figure 1e, the white phase is NMC, the gray phase is LTAP and the black phase includes both pore and

7

super-P carbon. The grayscale histogram (Figure 1d) of the image slice (Figure 1e)

shows three separated peaks, allowing automatic segmentation of the three phases.

Figure 1f shows the 3D reconstruction of the 700 psi LTAP-NMC electrode generated

by Avizo®, where white and gray colors represent NMC phase and LTAP phase

respectively.
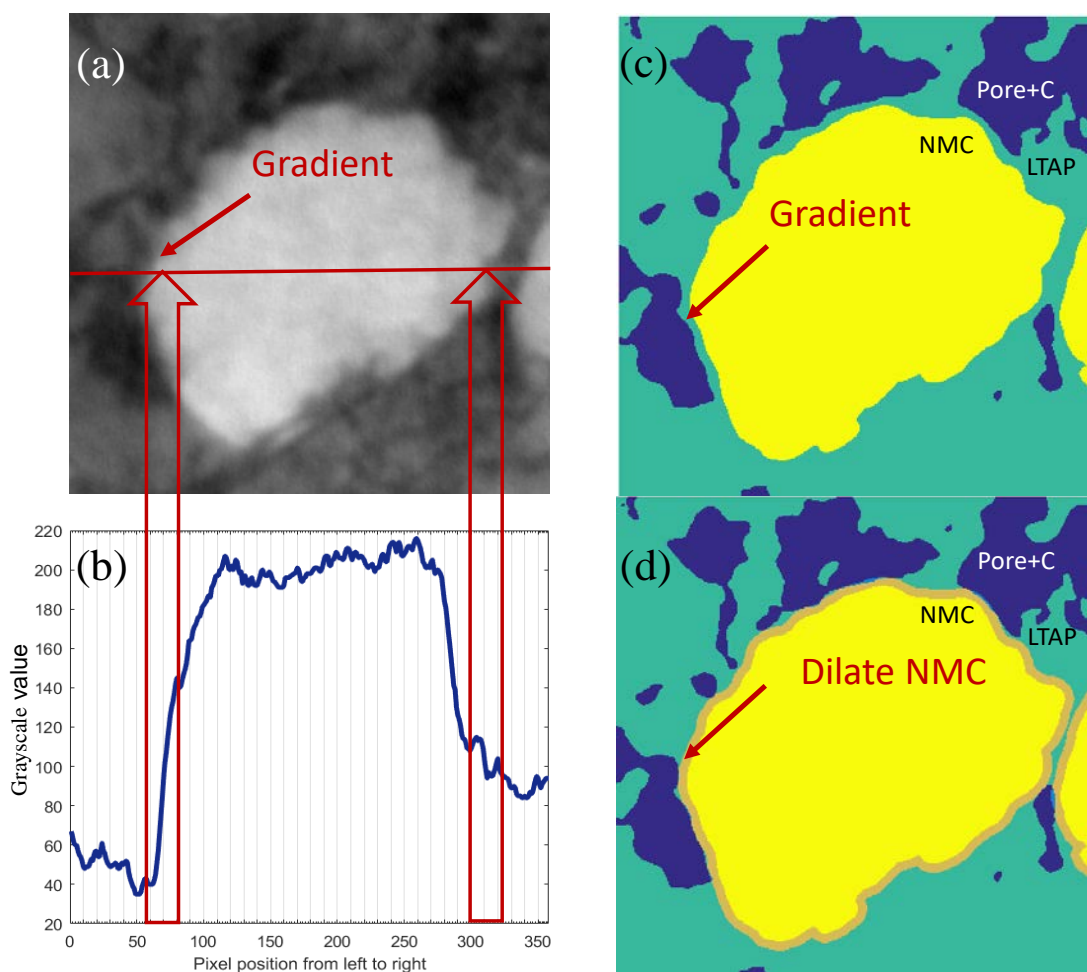
Figure 2. (a) A sample 2D CT image with NMC, LTAP and pore phases. (b) Grayscale

value variation on the red line in the CT image shown in (a). (c) Three-phase

segmentation using two thresholds. (d) Remove gradient by dilating NMC particles in

order to find contact interface between NMC and LTAP.

8

However, if there are more than two phases to be distinguished, the automatic

segmentation by simple threshold generates a thin film coating on the interface between

the white phase material and the black phase material. As shown in Figures 2a and b,

the arrow points a grayscale gradient at the interface between the white phase (NMC,

highest grayscale value) and the black phase (pore + carbon, lowest grayscale value)

on the red line in a 2D CT image. On the right side of the red line, there is an interface

between the white phase (NMC) and the gray phase (LTAP, grayscale value is in

between white phase and black phase). As shown in Figure 2b, the grayscale value of

the gray phase is always within the grayscale gradient at the interface between the white

phase and the black phase. The automatic segmentation by two thresholds generates a

ternary slice image as shown in Figure 2c, where the yellow color is NMC, green color

is LTAP and blue color is pore + carbon. The NMC particle is coated by a thin film of

LTAP due to the grayscale gradient at the interface between NMC and pore + carbon.

As a result, the contact between NMC and LTAP is always 100%, which is not real.

One way to address this problem is to do the segmentation manually, which could be

very time-consuming when hundreds of images need to be processed. In addition,

manual segmentation will generate random artifacts. In this work, a dilation algorithm

in Avizo® was used to remove the thin LTAP film coated on NMC particles. As shown

in Figure 2d, the NMC phase in the 2D ternary image was extended 3 pixels at the

boundary. After dilation, the thin LTAP film coated on NMC was replaced by the

extension of NMC phase. It should be noted that dilation will increase the size of NMC

9

particles and introduce a systematic error. The smaller the NMC particle is, the larger

the artifact is. As shown in Figure 2, the size of most of the NMC particles are in several

hundred pixels. Adding 3 pixels on the boundary will not affect accuracy significantly.
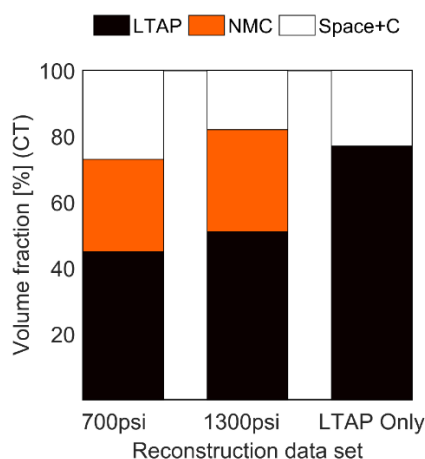

Figure 3. Volume fractions of the electrode components calculated from the

reconstructed porous microstructures.

To analyze the electrode geometrically, tetrahedral meshed microstructures of the

electrodes were generated from the ternary volumetric data with iso2mesh MATLAB

algorithm[30]. The reconstructed volumes used for geometrical analysis are around $25 \times$

25×25 μm^3. Figure 3 shows the volume fractions of the electrode components

calculated from the reconstructed porous microstructure of the all-solid electrodes and

the LTAP separator. As the pressing pressure increased from 700 psi to 1300 psi, the

volume fraction of pore + carbon is reduced from 27% to 18%. In the LTAP separator,

the volume fraction of pore is 23%. Compared with liquid electrolyte electrode, pore

phase does not contribute to Li ion conduction in all-solid LIB electrodes. Reducing the

volume fraction of pore phase can increase the ionic conductivity and the volumetric

10

energy density of all-solid LIBs. The possible approaches could be reducing the particle

size of LTAP solid electrolyte and increasing pressing pressure.

Table 1. LTAP and NMC contact and tortuosity of the all-solid electrodes under

different pressure and LTAP separator.

	Contact area/NMC surface area	Contact area/total NMC volume (1/um)	Tortuosity calculated from CT data	Tortuosity calculated from Bruggeman relation
LTAP			2.3	1.1
700 psi	55%	0.530	6.7	1.5
1300 psi	59%	0.622	4.6	1.4

The 3D reconstructed microstructures of 700 psi electrode, 1300 psi electrode and the

LTAP separator were quantitatively analyzed to characterize their geometric properties,

such as tortuosity and interfacial contact area between NMC and LTAP. The interfacial

contact area between NMC and LTAP is directly related to the intercalation reaction

during charge and discharge processes because the reaction occurs at the interface

between active material and solid electrolyte. The tortuosity is directly related to Li ion

transport in the electrode. As shown in Table 1, the LTAP phase only covers about 55%

of the NMC particles for the 700 psi sample. As the pressing pressure is increased to

1300 psi, the contact area is increased to 59%. The improvement is not significant and

it means that much higher pressure or smaller LTAP particles are required to achieve

larger contact area, thereby facilitating the intercalation reaction. Ion transport property

in a porous electrode could be quantified by tortuosity (τ). Tortuosity has been

11

considered as a function of porosity (ϵ) by Bruggeman relation $\tau = \epsilon^{-0.5}$. Evidence

has indicated that Bruggeman relation underestimates tortuosity in LIB electrodes [21, 27-

28]. Tortuosity in all-solid electrode cannot be calculated by Bruggeman relation because

there are three phases in the electrode and Li ion transports through the solid LTAP

phase. Instead, we can replace the porosity by the volume fraction of LTAP in the

Bruggeman relation. In this study, tortuosity was also calculated from the CT

microstructure using the method proposed by Kehrwald et al.[21]. The results in Table 1

show that Bruggeman relation significantly underestimates the tortuosity. The

tortuosity calculated from the CT data is 2 – 4 times of the values calculated from

Bruggeman relation. Compared with our previous publication on liquid electrolyte

LIBs, the tortuosity is also much higher. It means that it is difficult for Li ion to transport

through the network of LTAP particles in all-solid electrode. It should be noted that the

CT reconstruction cannot reveal the detailed features under the spatial resolution of

58.2 nm. It is very likely that the contact between particles is not seamless contact.

Points-like contact could be very possible and the tortuosity and Li transport will

deteriorate further. In addition, if the active material particles have volume changes

during cycling, the stability of the contact could be affected, leading to poor cycle life.

In summary, the 3D morphology of all-solid LIB electrodes was obtained and analyzed

by using Synchrotron TXM tomography with voxel size of $58.2 \times 58.2 \times 58.2$ nm^3 at

beamline 32-ID-C at the APS of ANL. A dilation method was used to solve the

grayscale gradient-induced problem in distinguishing three phases during

12

segmentation. The geometric analysis show that the contact between solid particles is limited even at 1300 psi pressing pressure, which significantly affect the Li ion transport in the electrode and the Li ion intercalation at the NMC/LTAP interface. In order to make the particle-based all-solid LIB feasible, the interface problem needs to be addressed.

13

References

1. Verma, P.; Maire, P.; Novak, P., A Review of the Features and Analyses of the Solid Electrolyte Interphase in Li-Ion Batteries. *Electrochimica Acta* **2010,** *55*, 6332-6341.

2. Knauth, P., Inorganic Solid Li Ion Conductors: An Overview. *Solid State Ionics* **2009,** *180*, 911-916.

3. Quartarone, E.; Mustarelli, P., Electrolytes for Solid-State Lithium Rechargeable Batteries: Recent Advances and Perspectives. *Chemical Society Reviews* **2011,** *40*, 2525-2540.

4. Fergus, J. W., Ceramic and Polymeric Solid Electrolytes for Lithium-Ion Batteries. *Journal of Power Sources* **2010,** *195*, 4554-4569.

5. Takada, K., Progress and Prospective of Solid-State Lithium Batteries. *Acta Materialia* **2013,** *61*, 759-770.

6. Wang, Y.; Richards, W. D.; Ong, S. P.; Miara, L. J.; Kim, J. C.; Mo, Y. F.; Ceder, G., Design Principles for Solid-State Lithium Superionic Conductors. *Nature Materials* **2015,** *14*, 1026-1031.

7. Ma, C.; Chi, M. F., Novel Solid Electrolytes for Li-Ion Batteries: A Perspective from Electron Microscopy Studies. *Frontiers in Energy Research* **2016,** *4*.

8. Sakuda, A.; Hayashi, A.; Tatsumisago, M., Intefacial Observation between LiCoO2 Electrode and Li2S-P2S5 Solid Electrolytes of All-Solid-State Lithium Secondary Batteries Using Transmission Electron Microscopy. *Chemistry of Materials* **2010,** *22*, 949-956.

9. Asl, N. M.; Keith, J.; Lim, C.; Zhu, L.; Kim, Y., Inorganic Solid/Organic Liquid Hybrid Electrolyte for Use in Li-Ion Battery. *Electrochimica Acta* **2012,** *79*, 8-16.

10. Zhu, Y. Z.; He, X. F.; Mo, Y. F., First Principles Study on Electrochemical and Chemical Stability of Solid Electrolyte-Electrode Interfaces in All-Solid-State Li-Ion Batteries. *Journal of Materials Chemistry A* **2016,** *4*, 3253-3266.

11. Woo, J. H.; Trevey, J. E.; Cavanagh, A. S.; Choi, Y. S.; Kim, S. C.; George, S. M.; Oh, K. H.; Lee, S. H., Nanoscale Interface Modification of LiCoO2 by Al2O3 Atomic Layer Deposition for Solid-State Li Batteries. *Journal of the Electrochemical Society* **2012,** *159*, A1120-A1124.

12. Seino, Y.; Ota, T.; Takada, K., High Rate Capabilities of All-Solid-State Lithium Secondary Batteries Using Li4Ti5O12-Coated LiNi0.8Co0.15Al0.05O2 and a Sulfide-Based Solid Electrolyte. *Journal of Power Sources* **2011,** *196*, 6488-6492.

13. Zaghib, K.; Armand, M.; Gauthier, M., Electrochemistry of Anodes in Solid-State Li-Ion Polymer Batteries. *Journal of the Electrochemical Society* **1998,** *145*, 3135-3140.

14. Prosini, P. P.; Mancini, R.; Petrucci, L.; Contini, V.; Villano, P., Li4Ti5O12 as Anode in All-Solid-State, Plastic, Lithium-Ion Batteries for Low-Power Applications. *Solid State Ionics* **2001,** *144*, 185-192.

15. Goodenough, J. B.; Kim, Y., Challenges for Rechargeable Li Batteries. *Chemistry of Materials* **2010,** *22*, 587-603.
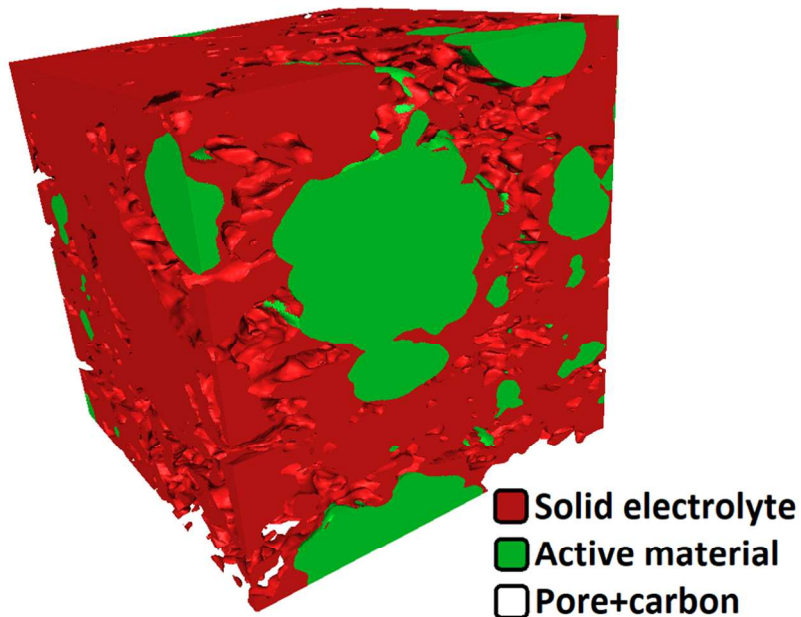
14

16. Hutzenlaub, T.; Thiele, S.; Zengerle, R.; Ziegler, C., Three-Dimensional Reconstruction of a LiCoO2 Li-Ion Battery Cathode. *Electrochemical and Solid State Letters* **2012,** *15*, A33-A36.

17. Wilson, J. R.; Cronin, J. S.; Barnett, S. A.; Harris, S. J., Measurement of Three-Dimensional Microstructure in a LiCoO$_2$ Positive Electrode. *Journal of Power Sources* **2011,** *196*, 3443-3447.

18. Stephenson, D. E.; Walker, B. C.; Skelton, C. B.; Gorzkowski, E. P.; Rowenhorst, D. J.; Wheeler, D. R., Modeling 3D Microstructure and Ion Transport in Porous Li-Ion Battery Electrodes. *Journal of The Electrochemical Society* **2011,** *158*, A781-A789.

19. Shearing, P. R.; Howard, L. E.; Jørgensen, P. S.; Brandon, N. P.; Harris, S. J., Characterization of the 3-Dimensional Microstructure of a Graphite Negative Electrode from a Li-Ion Battery. *Electrochemistry Communications* **2010,** *12*, 374-377.

20. Shearing, P. R.; Brandon, N. P.; Gelb, J.; Bradley, R.; Withers, P. J.; Marquis, A. J.; Cooper, S.; Harris, S. J., Multi Length Scale Microstructural Investigations of a Commercially Available Li-Ion Battery Electrode. *Journal of the Electrochemical Society* **2012,** *159*, A1023-A1027.

21. Kehrwald, D.; Shearing, P. R.; Brandon, N. P.; Sinha, P. K.; Harris, S. J., Local Tortuosity Inhomogeneities in a Lithium Battery Composite Electrode. *Journal of the Electrochemical Society* **2011,** *158*, A1393-A1399.

22. Liu, Z.; Chen-Wiegart, Y. C. K.; Wang, J.; Barnett, S. A.; Faber, K. T., Three-Phase 3D Reconstruction of a LiCoO2 Cathode via FIB-SEM Tomography. *Microscopy and Microanalysis* **2016,** *22*, 140-148.

23. Moroni, R.; Borner, M.; Zielke, L.; Schroeder, M.; Nowak, S.; Winter, M.; Manke, I.; Zengerle, R.; Thiele, S., Multi-Scale Correlative Tomography of a Li-Ion Battery Composite Cathode. *Scientific Reports* **2016,** *6*, 30109.

24. Chen-Wiegart, Y. C. K.; Liu, Z.; Faber, K. T.; Barnett, S. A.; Wang, J., 3D Analysis of a LiCoO2-Li(Ni1/3Mn1/3Co1/3)O-2 Li-Ion Battery Positive Electrode Using X-Ray Nano-Tomography. *Electrochemistry Communications* **2013,** *28*, 127-130.

25. Liu, Z.; Cronin, J. S.; Chen-Wiegart, Y. C. K.; Wilson, J. R.; Yakal-Kremski, K. J.; Wang, J.; Faber, K. T.; Barnett, S. A., Three-Dimensional Morphological Measurements of LiCoO2 and LiCoO2/Li (Ni1/3Mn1/3Co1/3)O-2 Lithium-Ion Battery Cathodes. *Journal of Power Sources* **2013,** *227*, 267-274.

26. Aono, H.; Sugimoto, E.; Sadaoka, Y.; Imanaka, N.; Adachi, G., Ionic-Conductivity of Solid Electrolytes Based on Lithium Titanium Phosphate. *Journal of the Electrochemical Society* **1990,** *137*, 1023-1027.

27. Kang, H. X.; Lim, C.; Li, T. Y.; Fu, Y. Z.; Yan, B.; Houston, N.; De Andrade, V.; De Carlo, F.; Zhu, L. K., Geometric and Electrochemical Characteristics of LiNi1/3Mn1/3Co1/3O2 Electrode with Different Calendering Conditions. *Electrochimica Acta* **2017,** *232*, 431-438.

28. Lim, C.; Yan, B.; Kang, H. X.; Song, Z. B.; Lee, W. C.; De Andrade, V.; De Carlo, F.; Yin, L. L.; Kim, Y.; Zhu, L. K., Analysis of Geometric and Electrochemical

15

Characteristics of Lithium Cobalt Oxide Electrode with Different Packing Densities. *Journal of Power Sources* **2016,** *328*, 46-55.

29. Lim, C.; Yan, B.; Yin, L.; Zhu, L., Geometric Characteristics of Three Dimensional Reconstructed Anode Electrodes of Lithium Ion Batteries. *Energies* **2014,** *7*, 2558-2572.

30. Fang, Q. Q.; Boas, D. A., Tetrahedral Mesh Generation from Volumetric Binary and Grayscale Images," *2009 IEEE International Symposium on Biomedical Imaging: From Nano to Macro*, Boston, MA, **2009**, 1142-1145.

16

1
2
3
4
5
6
7
8
9
10
11
12
13
14
15
16
17
18
19
20
21
22
23
24
25
26
27
28
29
30
31
32
33
34
35
36
37
38
39
40
41
42
43
44
45
46
47
48
49
50
51
52
53
54
55
56
57
58
59
60

266x190mm (119 x 119 DPI)